

A Hybrid Medical Image Denoising based on Block Matching 3D Collaborative Filtering

Ambika Annavarapu (✉ ambiannavarapu@gmail.com)

K.S. Institute of Technology, Visvesvaraya Technological University

Surekha Borra

K.S. Institute of Technology

Vijay Bhaskar Reddy Dinnepu

AgWiQ Technologies Pvt Ltd

Mankamana Prasad Mishra

Cisco Systems (United States)

Research Article

Keywords: Block Matching, Collaborative filtering, Contrast - to - Noise – Ratio, Richardson_Lucy Algorithm, Rudin_Osher_Fatemi model, Peak - Signal - to - Noise - Ratio

Posted Date: May 6th, 2022

DOI: <https://doi.org/10.21203/rs.3.rs-1607385/v1>

License:  This work is licensed under a Creative Commons Attribution 4.0 International License.

[Read Full License](#)

A Hybrid Medical Image Denoising based on Block Matching 3D Collaborative Filtering

*¹Ambika Annavarapu, ²Surekha Borra, ³Vijay Bhaskar Reddy Dinnepu, ⁴Mankamana Prasad Mishra

*¹Research Scholar, Department of ECE, K.S. Institute of Technology, Visvesvaraya Technological University, Belagavi, Karnataka, India, ambiannavarapu@gmail.com,
ORCID: 0000 – 0002 – 7684 – 2162

²Professor, Department of ECE, K.S. Institute of Technology, Bangalore, India,
borrasurekha@gmail.com

³Founder and CEO, AgWiQ Technologies Pvt Ltd, Bangalore, India, vijaybrd@gmail.com

⁴Cisco systems, 1853 Camacho way , San Jose 9513, **United States** Mankamis@cisco.com

Corresponding author: ambiannavarapu@gmail.com, ORCID: 0000 – 0002 – 7684 - 2162

Abstract: To mitigate the noise effects without information loss at the edges of the radiological images, a well-designed preprocessing algorithm is required to assist the Radiologists. This paper proposes a hybrid adaptive preprocessing algorithm that utilizes a Rudin_Osher_Fatemi (R_O_F) model for edge detection, Richardson_Lucy (R_L) Algorithm for Image Enhancement, and Block Matching 3D Collaborative filtering for denoising of image. The performance of the proposed method is assessed and estimated on two realistic datasets, one on chest X-ray images and the another on MRI/CT images. The proposed hybrid system verifies the data reliability of Gaussian noise affected medical images. The simulation results shows that the proposed adaptive method attains a high value of Peak Signal-to-Noise ratio of 47.4433 dB for chest X-Ray and 46.8674 dB for MRI/CT datasets respectively at a standard deviation value of 2. Performance analysis of the proposed scheme is further carried out using various statistical parameters of Root Mean Square Error, Contrast – to – Noise ratio, Bhattacharya Coefficient and Edge Preservation Index. A comparative analysis on denoised image quality shows that the proposed system achieves better performance than several existing denoising methods.

Keywords: Block Matching, Collaborative filtering, Contrast - to - Noise – Ratio, Richardson_Lucy Algorithm, Rudin_Osher_Fatemi model, Peak - Signal - to - Noise - Ratio

1. Introduction

Today image processing [1] is believed to be the most challenging, as images are rich at information in the fields like medicine, space, RADAR, machine vision, etc. Rapid growth in the computer technology enables the performance of the image processing methods by improving the quality of the images acquired by various medical imaging systems. Often, noise affects the images during image acquisition, storage, and transmission, which is undesirable. Denoising of

image aims at restoring the original image from noisy image by removing the noise, but at the same time retaining the quality of high frequency components like texture and edge. To diminish the noise effect in medical-images, researchers have implemented various denoising algorithms whose performance relies on various parameters like Peak – Signal – to – Noise ratio, Contrast – to – Noise ratio, Root Mean Square Error, Bhattacharya Coefficient, and Edge Preservation Index at various values of standard Deviation. Denoising of medical images [2] is generally grouped into four categories: filtering, transform domain denoising, machine learning based denoising and statistical domain based denoising. Denoising of medical images using filtering-based methods is carried out using linear [3-4] and non-linear [5-6] filtering methods in spatial domain, which usually results in information loss at the edges. To overcome this drawback, transform domain based denoising approaches are considered. This category of techniques performs the denoising in various domains of wavelet [7], Curvelet [8], Contourlet [9] and Fast Fourier Transform [10]. As the image size increases, the performance of this domain decreases exponentially. This snag can be overcome by considering the machine learning based denoising approaches which includes bioinspired systems like Boltzmann Machines [11-12], autoencoders [13], Convolutional Neural Networks [14-15], Genetic algorithms [16-20], etc. The major mitigation of these techniques is the computational complexity, due to involvement of image processing globally. This drawback can be avoided with the help of statistical approaches [21-27], which can be employed with a lesser amount of complexity and less computational time. Various drawbacks of these basic denoising methodologies can be resolved with adaptive methodologies like Block-Matching and 3D filtering (BM3D) algorithm.

BM3D) algorithm, developed by Dabov, K., et al. [28] improved the denoising by enhancing the sparsity of the transform. The blocks are processed in a sliding manner in an image to search for the required similar blocks from a pile of blocks in order to arrange a 3D array. The noise is reduced by reducing the 3D-decorrelating unitary transform coefficients. All the matched blocks estimates are then obtained by applying inverse 3D transform. The capability of this method to preserve the textures is tested on the heavily noisy (Standard Deviation, $\sigma = 100$) Barbara image and found that this method can be applicable only for fixed-sized blocks.

Dabov, K., et al. [29] enhanced the BM3D approach by combining it with Collaborative-filtering to improve the sparsity generated by grouping the matched blocks. Three steps are involved: 3D-transform application on a group, the transform-spectrum shrinkage, application of inverse 3D-transform. This results in 3D-estimate of image blocks that are jointly filtered. Collaborative-filtering exposes finest-details of all the shared grouped-blocks and preserves features of all the individual blocks. Performance of this method is enhanced by considering the Wiener filtering.

Later, to exploit non-local image modeling. Dabov K., et al. [30] implemented an adaptive BM3D approach using Principal-Component Analysis as well as local-Shape adaptive-anisotropic estimation. The denoising method is performed using spectrum-shrinkage of a 3D-transform that is applicable to these groups. The shrinkage effect mainly relies on transform capability to separate it from noise. Sparsity in the proposed method is enhanced by applying Principal-Component Analysis on neighborhoods that contains adaptive-data shape. Bases of this

Principal-Component Analysis are found by Eigen value-decomposition of matrices having empirical second moments.

To improve the algorithm performance for high noise affected images, Chen, Q., et al. [31] introduced a two-folded bounded BM3D algorithm where in the image is first partitioned into multiple-regions to identify the boundaries among the regions. The block-matching is performed inside this template-block region. Secondly, to avoid the loss of edges by collaborative-filtering, a partial-block matching for various block-coherent segments of multiple regions is performed. This method enhanced PSNR value to 0.23 from 1.33 dB compared to the general BM3D. Lebrun, M. [32] improvised the transparency of the BM3D algorithm by considering the new notation which works with spatial dimensions along with the third dimension. This method is an adaptive BM3D algorithm in an open-source approach, where in the spatial dimensions are also considered to retrieve the lost details during edge contrasting. A low maximum-number of identical patches is stored to choose various parameter values. This model is improved by considering the weighting-contingent that depends on standard deviation of various 3D-estimated groups and also by applying ideal-Wiener filter. This method is slow, complex and less-flexible than the fundamental methods and also results in artifacts at high noise levels.

Burger, H. C., et al. [33] associated BM3D algorithm with a plain Multi-Layer Perceptron to apply the algorithm to large sized image patches. This approach is proposed for less-extensively used noises. Large network capacity, large patch-size and large training-set are considered for this denoising approach. These parameters can be achieved by applying plain Multi-Layer Perceptrons on GPUs that are used to train as well as to apply various neural networks. But this approach can be applied only on single noise level when $\sigma \geq 25$. Zhong, H., et al. [34] performed non-local centralization prior to the usage of wavelet-coefficients local-sparsity. The 1D-transformed inter-blocks are removed to establish a nonlocal-centralization based on grouped-blocks nonlocal-similarity as well as local-sparsity of different wavelet-coefficients. Three nonlocal-shrinkage functions are introduced in this method by considering norm restrictions of inter-blocks of wavelet coefficients along with intra-blocks of wavelet coefficients.

Sarjanoja, S., et al. [35] implemented the BM3D algorithm on heterogeneous computer-platforms using CUDA and OpenCL methods and enhanced the calculation speed to a rate of 7.5 times than the CPU implementation. This method utilizes parallel processing in various heterogeneous platforms for implementing existing approaches of denoising. These implementations are tested on various testing images affected by synthetic or natural noise. This method mainly focused on improving the speed of implementation to 1.5 times. The challenges faced by this method are related to memory usage and serialization of accessed data.

Li, Y., et al. [36] implemented BM3D along with the Total Variation method to perform self-adaptation when the amount of noise is varied, and to reduce the implementation time. Total Variation based framework is proposed to estimate the noise to get the references to execute the self-adaptation. Another problem faced by BM3D during denoising is computational time required to search the similar blocks. This shortcoming is overcome by the hybrid denoising

approach that utilizes a novel Total_Variation based BM3D approach. Hasan, M., et al. [37] enhanced the BM3D performance by focusing on improvement of Structural Similarity Index value instead of reducing the Mean Square Error value. Wiener filtering is improved by achieving the maximum Structural Similarity amid estimated and true image, rather than minimizing the value of Mean Square Error. A 3D based zigzag thresholding is introduced to improve the DC only based BM3D profile.

Existing methods to perform collaborative filtering used uncomplicated approximations for the transform of noise-power spectrum. These techniques do not consider the block matching which causes the inaccurate results while denoising the noise affected images. Mäkinen, Y., et al. [38] introduced a framework for effective approximations and exact computations. In this method, the noise variance in block is correlated with the other similar blocks to extract the accurate noise power spectrum inside shrinkage. This results in accurate values in block matching as well as in aggregation.

Wang, H., et al. [39] introduced an adaptive local-similarity in BM3D method, which uses the redundant data on similar image-patches. General BM3D approach can be applied for conventional images only, but not for the images that are having complex structures. When BM3D is applied to these complex structures, the particulars about images are damaged, as well as it lessens the factor of reflected signal fidelity. These drawbacks can be overcome by the model, which recovers the signal energy leaking that is affected by noise. This model enhanced the performance of the denoising, by improving the Signal-to-Noise Ratio.

Zhao, T., et al. [40] enhanced the Gaussian noise affected Computed Tomography images to thrust boundary of ALARA. The post thresholding signal in transform domain is applied by Wiener filtering to enhance the denoising. The Minimum-Mean Square Error criteria-based Wiener filter is considered to get the optimal transform domain coefficients, considering the noise/signal cross-spectrum and noise-spectrum. In this method, an ultra-low-dose and full-dose image datasets are considered to estimate the performance of denoising. Peak - Signal - to - Noise - Ratio along with Emphysema is considered as performance metrics of denoising.

Yahya, A. A., et al. [41] proposed an adaptive filtering based BM3D approach to enhance the denoising capability without damaging the image details. Hard-Thresholding used in BM3D is replaced by adaptive filtering in this model to adapt and modify according to the amount of noise. In this algorithm, total variation-based method is validated to low-noise affected areas, while soft-thresholding is applicable to various areas in an image that are prone to high-noise. This method enhances the stability and self-adaptation by resulting in optimal noise reduction. An adaptive threshold is considered to avoid the noise due to lower thresholds and loss of image details due to higher threshold values. Additionally, an adaptive-weighted function is considered to evaluate the spatial distance among candidate patches and reference patch. If this distance is small, a dissimilarity measurement is evaluated, whereas, if the distance is large, a k-means clustering is computed.

Hanchate, V., et al. [42] used Noise-Invalidation denoising method and Variance-Stabilization Transform along with BM3D to denoise the Magnetic Resonance Images. Hard-thresholding in

BM3D is replaced by Noise-Invalidation approach to give the automatic threshold based on the noise levels and image characteristics like image wavelet-coefficient. Prior to the denoising using BM3D, a Variance stabilization transform is applied to mitigate the noise-variance dependency. To improve the performance metrics further, the denoised image is subjected to Contrast-Limited-Adaptive-Histogram-Equalization. Esedoğlu, S., et al. [43] introduced an anisotropic version for noise removal and edge preservation depending on Total Variation model developed by Rudin, Fatemi and Osher. Convex regions with desired shapes are considered to evaluate the model. Properties of various minimizers are studied to investigate anisotropic energies and indicator functions that can exhibit exact solutions and to identify the general conditions in isotropic case.

Aubert, G., et al. [44] implemented a variational approach based on numerical study of noise reduction and preservation of image textures proposed by Rudin, Fatemi and Osher. The minimization of energy functions in this mode is by classifying an image into two components. The Binary Variation is the first component that is used to get the geometrical information of image, whereas, second component consists of signals with large oscillations like textures and noise. The functional analysis arguments based on harmonic analysis tools are considered in bounded regions, to study the energy functions that are used to retrieve the image components. Further, various numerical experimentations are executed to show the significance of this proposed model in both denoising of image and image decomposition methods.

Haddad, A., et al. [45] improved the Rudin_Osher_Fatemi (R_O_F) based denoising methods of image by considering various mathematical properties, to split textures and image objects. The energy function in the proposed approach is minimized by considering the “dual norm” concept. Both the stability and invariance concepts are considered to characterize the simple class functions named as, extremal functions. In this model, Binary Variation is considered to improve the R_O_F method by cancelling all the texture components. These extremal functions are helpful in demonstrating the lack of uniqueness during optimal decomposition. Chambolle, A., et al. [46] discussed the mathematical analysis of image reconstruction based on Total_Variation in both practical and theoretical ways. Firstly, minimization functions based on theoretical approach is studied using perimeter minimization and R_O_F approach. Secondly, various applications are addresses based on Total_Variation like image deblurring and zooming; using data fidelity term; nonconvex data problems; and minimum partition problem.

Getreuer, P [47] implemented the denoising of a Gaussian noise affected image by using a total_variation regularization approach. Bregman_Iteration is considered to solve constrained-convex minimization problems, whereas Split-Bregman is considered for the non-differentiable-convex minimization problems. Then a discrete-derivatives framework is applied to handle the uniformly sampled functions. To balance the denoising of image and to avoid image details, a tuning approach is considered to optimize the parameters. Said, A. B., et al. [48] proposed a total variation based denoising approach to preserve the image edges. General R_O_F model using gradient regularizer results in loss of image information and a staircasing-effect. To overcome this drawback, an adaptive edge detector is introduced along with non-local mean filter, structure

tensor and fuzzy component. This approach gives low denoising at edges, and high denoising at smooth regions.

Phan, T. D. K [49] proposed an adaptive image-surface-mean curvature based R_O_F model to control the smoothing strength and has analytically studied the structure convergence. Further, numerical-realization is carried out by Split-Bregman approach. Gaussian noise elimination as well as the edge preservation is balanced and at every level of estimated images, a new formula is introduced to estimate the level of noise. The optimization problem is resolved using Split-Bregman approach and its performance is evaluated quantitatively and qualitatively with respect to existing variational based approaches. Fish, D. A., et al. [50] extended Richardson_Lucy (R_L) method based on blind-deconvolution and the algorithm performance was compared with the existing Wiener-filter based blind-deconvolution algorithms. Further, various Point_Spread functions based functional forms are considered to evaluate the parameters that are unknown. This algorithm has high noise tolerance levels compared to existing blind-deconvolution approaches.

Dell'Acqua, F., et al. [51] introduced spherical deconvolution based damped version of R_L algorithm to denoise the diffused MRI images. General convolution approaches cannot avoid the degradation of the spherical-deconvolution results of the isotropic tissue. To avoid this drawback, an adaptive-regularization algorithm is introduced and is applied to both vivo and stimulated datasets and the obtained results are evaluated to match standard-negative-constrained framework. The R_L framework reduces the false fiber-orientations and also conserves the main-fibre orientations angular-resolution. The algorithm requires less scan-time and high-speed of processing.

Yongpan, W., et al. [52] introduced an adaptive R_L algorithm to improve the ringing artifact present in image-deconvolution. A local-prior approach is considered in the R_L algorithm to avoid the ringing artifact obtained because of the failure of blur-kernel estimation. Firstly, the standard-deviation of the local-window pixels are evaluated to obtain the smooth-region. Secondly, a new mask is introduced to avoid the ringing-artifact at the image edges. This step plays a significant role if the image has a rigid foreground and smoothing background. Thirdly, if the boundary is smooth, then a boundary-constraint is applied.

Tam, N. W., et al. [53] introduced a Haar-Wavelet transform based R_L technique to reinstate Positron Emitted Tomography images. The approach considers spatially variant Point Spread Functions to enhance the image quality. The Coefficient Variation and Contrast Recovery parameters are considered to estimate the proposed method performance. The resolution of the images is recovered in this approach without increase in the number of iterations and without increase in noise levels. Wu, J. L., et al. [54] introduced an edge-map based R_L algorithm to avoid the motion-blur artifacts in images. The noise affected image is divided into edge as well as smooth regions prior to the deconvolution process. Local-extrema filtering is utilized to extract the information of edge-map of the image that contains the smooth regions. Each iteration of this deconvolution process reduces the ringing-artifact gradually. This adaptive algorithm reduces the ringing-artifact while preserving the information of the image edges.

Similarly, Yang, H. L., et al. [55] proposed a Gradient-Attention based R_L algorithm and a bilateral-filtering based blur-kernel estimation in addition to non-blind-image deconvolution to reduce the blur due to motion in an image. In blur kernel estimation, an alternating kernel refinement course is considered to get an unclear image using quadratic-regularization based method. In this non-blind based image deconvolution process, image gradients and Gradient Attenuation R_L algorithm are considered to identify the ringing artifact in R_L algorithm. The performance of this adaptive framework is evaluated by different real datasets.

Chen, D., et al. [56] implemented R_L algorithm along with Kirchhoff approximation and Multi-Gaussian-Beam modeling to improve image restoration of simulated-C Scan images. This adaptive algorithm improves the Point Spread Functions that are obtained using Multi Gaussian Beam Model. The final iteration number is obtained by deriving a relation amid inclusion of size of an image and final iteration number. The effect of Electromechanical change and sound attenuation gives the correction factor size. The performance of this adaptive method is evaluated using optical micrograph results.

From the literature [57-61], it is observed that while sparsity is much improved by BM3D algorithm, poor performance is resulted at textural regions and sharp edges, at high noise levels. Even though BM3D results in excellent denoising performance, it is not suitable for the images affected with high noise levels. To overcome this hitch, this paper proposed a hybrid denoising algorithm. The Gaussian noise affected Magnetic Resonance Image is applied to R_O_F algorithm for edge detection, followed by image denoising using BM3D approach. Later, the denoised image is applied to R_L algorithm for image enhancement.

The rest of the article is ordered as follows. Section 2 provides the preliminaries, section 3 proposes the hybrid denoising methodology, section 4 overviews the statistical parameters used for performance evaluation. Section 5 discusses the results generated by the proposed adaptive approach. Section 6 gives the conclusion along with the future scope of the paper.

2. Preliminaries

2.1. Hard-Thresholding

Hard thresholding is an optimal threshold used to eliminate noise in images. This can be achieved by using a feedback to optimize the threshold value each time. Before applying the hard thresholding to gray-level medical images, consider log-based transformation to enhance the image quality.

$$P = c * \log(1 + p) \tag{1}$$

where c is the constant based on the amount of image enhancement, p is the input pixel value and P represents the output pixel value. After applying the threshold, perform the inverse log-transformation. Before converting the image from gray-scale to binary, set threshold to each pixel. The algorithm for hard-thresholding is represented below

Input: Medical-image affected by Gaussian noise.

Output: Denoised medical image

Step 1: Consider a gray-scale image

Step 2: Select an initial threshold value Th .

$$Th = \sigma^2 \sqrt{2 \log S} \quad (2)$$

where σ is the noise standard deviation, S is the image size.

Step 3: Divide the image into two components

Step 3.1: If the pixel value is less than or equal to threshold, then consider it as background.

Step 3.2: If the pixel value is greater than threshold, then consider it as foreground.

Step 4: Evaluate Mean value of foreground and background images.

Step 5: Consider a new threshold value by performing the average of two mean values.

Step 6: If the difference between old and new threshold values is less than a pre-assigned limit, stop the procedure or else repeat steps 2 to 6.

2.2. Wiener filtering

Wiener filtering removes the Gaussian noise from the noise affected images, where its statistics of estimation depends on neighboring pixels. Wiener filter relies on the noise strength i.e. amount of noise contrast. Amount of smoothing in Wiener filter linearly varies on the noise contrast. It can also be applied in the frequency band during image corruption due to noise. Mathematical representation of Wiener filter is given as

$$I(m, n) = N(m, n)W(m, n) \quad (3)$$

where $N(m, n) = \frac{P_W(m, n)}{P_W(m, n) + \sigma^2}$; $\sigma^2 = \frac{1}{k^2} \sum_{m=1}^k \sum_{n=1}^k N^2(m, n) - \mu^2$; $\mu = \frac{1}{k} \sum_{m=1}^k \sum_{n=1}^k N(m, n)$

$W(m, n)$ is the Fourier spectrum of Wiener filter, $I(m, n)$ is the original image spectrum, $N(m, n)$ is the noise affected image spectrum, and $P_W(m, n)$ is the noise power spectrum of the noise.

Coefficients of Wiener filter are evaluated by minimizing the square of the distance between required signal and filter output.

2.3. Rudin_Osher_Fatemi (R_O_F) Model

R_O_F is a time-dependent Partial Differential Equation model that uses numerical algorithm based on constrained optimization of images. Traditional methods use simulated annealing approach to obtain the minimization, which is a computationally slow approach. To avoid this drawback, the R_O_F approach considers the local extrema that minimizes the image total variation depending on constraints like noise statistics. These constraints are imposed based on Lagrange multipliers. The solution of time dependent Partial Differential Equation is obtained by using an approach named gradient projection technique.

A simple geometric description-based image is considered to apply the R_O_F algorithm, which contains the objects, a set of connected sets, smooth edges, or contours. The image contains jumps around the boundaries, and smooth inside the objects which are considered as bounded variation functions. These models which are dependent on total variation works poorly with the images containing oscillatory components like fine structures and textures. The mathematical evaluation of the R_O_F approach is as follows.

Let the image be i and the noise affected image be d . The relation between these two images is given as in equation (4)

$$d = Ri + n \quad (4)$$

where R is a linear-operator that is used for modeling blur and n is the noise. Minimization of energy is a solution to this problem. Energy consists of two terms, namely, regularization of cost function as well as fidelity term. This model depends on the assumption of Bounded Variation ($BVA(\Omega)$), where Ω is the domain. Reconstruction of the original image i is obtained by using conventional method of Least-Squares L^2 fit leading to linear equations. The image is decomposed into a component i that belongs to $BVA(\Omega)$ and a noise component n which belongs to $L^2(\Omega)$. In the two-dimensional continuous system, the constrained minimization problem is represented as in equation (5)

$$\inf_{(i,n) \in BVA(\Omega) \times \frac{L^2(\Omega)}{d} = i+n} \left(\int |\nabla i| + \frac{\lambda}{2} |Ri - d|^2 \right) \quad (5)$$

for a positive value of LaGrange-Multiplier λ , subject to the constraints of mean $\int_{\Omega} Ri$ and a standard deviation of $\int_{\Omega} |Ri - d|^2 = \sigma^2$.

Limitations of this model rely on the boundary conditions. Consider functions (ϕ) in the space (C') functions from Ω to M^2 with the help of compact support i.e. $[C'_0(\Omega)]^2$. Variance of this function $i \in L'(\Omega)$ is defined as in equation (6)

$$|u|_{BVA} = \int_{\Omega} |\nabla i| = \sup_{\phi \in [C'_0(\Omega)]^2, |\phi| \leq 1 \text{ Point-wise}} \int_{\Omega} i \nabla \cdot \phi \quad (6)$$

The discrete energy of this minimize is given by equation (7)

$$E_m(i) = \sum_{a,b=0}^{m-1} \mu_{a,b} |(\nabla i)_{a,b}| + \frac{1}{2\lambda} \sum_{a,b=0}^{m-1} \mu_{a,b} (i_{a,b} - d_{a,b})^2 \quad (7)$$

where $(\nabla i)_{a,b}$ is a two-dimensional function that can be represented as in equation (8)

$$(\nabla i)_{a,b} = \left((\nabla_x i)_{a,b}, (\nabla_y i)_{a,b} \right) \quad (8)$$

where $(\nabla_x i)_{a,b} = \frac{i_{a+1,b} - i_{a,b}}{p}$ and $(\nabla_y i)_{a,b} = \frac{i_{a,b+1} - i_{a,b}}{p}$, where $p = 1/m$

This function satisfies the Neumann-Boundary conditions as represented in equation (9)

$$\begin{aligned} i_{-1,b} &= i_{0,b} & i_{m,b} &= i_{m-1,b} \\ i_{a,-1} &= i_{a,0} & i_{a,m} &= i_{a,m-1} \end{aligned} \quad (9)$$

The R_O_F algorithm is summarized as below:

Input: Medical image affected by Gaussian noise.

Output: Edge detected image

Step 1: Consider a noise affected image 'd' assuming 'i' as input noise free image.

Step 2: Minimize the energy equation represented using equation (3) and by equation (4) in the discrete case depending on the Boundary_Variation.

Step 3: If the minimized energy value does not satisfy the Neumann-Boundary conditions as shown in equation (6), then repeat step 2.

Step 4: If the minimized energy value satisfies the Neumann-Boundary conditions, then the edge of the region is obtained.

Step 5: Repeat step 2 to detect image 'i' edges.

2.4. Block Matching 3D Filtering (BM3D)

BM3D [28] initially proposed by Dabov et al. [29] for denoising was improved by Lebrun [32] to enhance the performance for Additive-White Gaussian Noise. BM3D algorithm is a two-step process of finding identical patches, similar to performing Non-Local Means filtering approach with a variation in the component. While the first step uses Hard-Thresholding, Wiener-Filtering is utilized in second step. BM3D first divides the noisy image into multiple patches or blocks. For each block, it produces a window that contains reference patch at its center. Later, a threshold value is used to find patches identical to the reference patch. A 3D block is constructed on grouping all the identical patches. Various transforms are applied to convert from spatial-domain to frequency-domain followed by hard-thresholding. The basic estimate is generated by converting the block coefficients into intensity values, by means of Inverse 3D transform. An aggregation is applied to the reference patch estimate to predict each pixel value. This basic estimate is applied to the BM3D second step as an oracle to perform 3D grouping. In this step, instead of Hard-Thresholding, the Wiener-filtering approach is used. The 3D group generated based on noisy affected image is considered as degraded image function and the 3D group which was constructed depending on basic estimate that is regarded as the degradation function.

The procedure to implement BM3D approach is summarized as follows:

Input: Noisy image

Output: Denoised medical image

Step 1: Find Basic Estimate

Step 1.1: Group Similar type of blocks as a 3D array

Step 1.2: Apply 3-dimensional transform is applied on the groups to transform from spatial domain to frequency domain.

Step 1.3: Reduce the noise from the transformed coefficients using a Hard Thresholding approach.

Step 1.4: Apply Inverse 3D Transform to estimate the coefficients

Step 1.5: Obtain basic estimate by weighing the estimates of all the overlapping block-wise estimates.

Step 2: Find Final Estimate

Step 2.1: Group similar type of blocks as a 3D array

Step 2.2: Apply 3-dimensional transform on the groups to transform from spatial domain to frequency domain.

Step 2.3: Apply Collaborative Wiener Filtering on the basic estimate of noisy energy-spectrum with basic estimate as a pilot signal.

Step 2.4: Group the Estimates of the blocks by applying an inverse 3-Dimensional transform.

Step 2.5: Compute original image final estimates by collecting local estimates with the help of a weighted average.

The aggregated weight generated after the aggregation technique gives the working of Wiener-filtering and is defined as follows:

$$\omega_b(\varepsilon) = \frac{|\tau_{BM}^w P^{ba}(P)(\varepsilon)|^2}{|\tau_{BM}^w P^{ba}(P)(\varepsilon)|^2 + \sigma^2} \cdot \tau_{BM}^w P(P) \quad (10)$$

where $P^{ba}(P)(\varepsilon)$ is the basic image 3-dimensional block and $P(P)$ is the noise image 3-dimensional block; τ_{BM}^w is the Wiener-filter phase 3-dimensional transformation and $\omega_b(\varepsilon)$ gives the weighted-aggregation operation.

2.5 Richardson-Lucy (R_L) Approach

R_L algorithm or Expectation-Maximum approach is an iterative algorithm that uses Point Spread Functions (PSF) to compute the reflective function of an object in an image. PSF represents the system response and decides image quality. The PSF represents the spatial domain version of image transfer function. Convolution between PSF and original object symbolizes the image of an item. R_L algorithm converge the iteration result to obtain a maximum-likelihood solution. This algorithm is mainly related to the images that follow Poisson distribution. Two main properties of R_L algorithm are energy preserving and non-negativity, which enhances the performance of the approach. Non-negativity of R_L algorithm constrains the expected values and conserves the energy of an image during iteration. The performance of the R_L algorithm is also enhanced because it requires only two multiplications and two convolutions per iteration. As the number of iterations increases, both the ringing artifacts and signal magnitude increases.

R_L algorithm begins with first estimate that consists of an observed image. It calculates a correction factor of every pixel that is multiplied with the pixel at every iteration. The value of the correction factor reaches to a value of '1' at the desired deconvolved image. Images are formed from the correction factors of pixels by applying convolution between PSF and current estimate, and then partition the observed image pixel-by-pixel using blurred estimate.

Richardson-Lucy algorithm is basically derived from Baye's theorem and produces high quality images depending on the maximum-likelihood implementation in the presence of high noises. The statistical fluctuations in an image are considered as the conditional probability values in the Baye's theorem as shown in equation (11) to reconstruct the noise affected images

$$P(a/b) = \frac{P(b/a)P(a)}{\int P(b/a)P(a)da} \quad (11)$$

where $P(a/b)$ is the event a conditional-probability with respect to event b. $P(a)$ gives the event a probability, and $P(b/a)$ gives the event b conditional-probability, with respect to event a. In R_L algorithm $P(a)$ is replaced by the object distribution $O(a)$, $P(b/a)$ by the Point_Spread Function centered around a, $PSF(b, a)$, and $P(b)$ by the degraded image $d(b)$. The R_L iterative algorithm is then given as in equation (12)

$$o_{i+1}(a) = \int \frac{PSF(b,a)d(b)db}{\int PSF(b,c)o_i(a)dc} o_i(a) \quad (12)$$

where i gives the number of iterations. Depending on the isoplanatic condition, equation (11) can be rewritten in terms of convolutions as in equation (13)

$$o_{i+1}(a) = \left\{ \left[\frac{d(b)}{[o_i(a) \otimes \text{PSF}(a)]} \right] \otimes \text{PSF}(-a) \right\} o_i(a) \quad (13)$$

where \otimes is the convolution operator. With a known $\text{PSF}(a)$ value, $o_{i+1}(a)$ can be evaluated by convergence. R_L algorithm can be started by estimating the initial value of $o_0(a)$ and the value in the subsequent iterations is highly deviated from the true value. Convergence achieved by the R_L algorithm attains sparse solutions, which are positive in the spatial domain reconstruction. R_L method is applied directly to the sparse coefficients instead of the subsequent images, to improve the sparsity of the images.

The R_L algorithm is summarized as below:

Input: Denoised medical image.

Output: Enhanced medical image

Step 1: Perform convolution of noise affected image with a known Point Spread Function (PSF)

Step 2: Attain the convex loss function represented in equation (12) using the Baye's theorem represented in equation (11).

Step 3: Minimize (or converge) the convex loss function to minimize the effect of noise on image by considering PSF of the image to be convoluted with the blurred image in order to obtain noise free image.

Step 4: Repeat step 3 until the value of $o_{i+1}(a)$ equals to $o_i(a)$, i.e., $o_{i+1}(a)$ is a minimum value.

3. Methodology

Application of BM3D algorithm alone for noise removal results in poor performance at high noise levels and for DC-only profile while denoising of medical-images. To overcome this problem, this article proposes a hybrid adaptive preprocessing algorithm which is based on Rudin_Osher_Fatemi model for edge detection, Richardson_Lucy Algorithm for Image Enhancement, and Block Matching 3D Collaborative filtering for denoising of image. The flowchart for this hybrid algorithm is presented in Fig. 1, and the steps involved in the proposed hybrid model are listed below:

Input: Medical-image affected by Gaussian noise.

Output: Denoised medical image

Step 1: Apply Rudin_Osher_Fatemi model to smoothen the edges of the images using linear soothing approach.

Step 2: If the degree of smoothness is as per requirement, perform denoising of images, or else repeat Step 1.

Step 3: Group the identical patches.

Step 4: Apply 3-dimesional transform to the patches.

Step 5: Start the denoising process by applying Hard thresholding to these patches.

Step 6: Convert the block coefficients into intensity values by applying a 3-dimensional inverse transform.

Step 7: Aggregate by making reference patch estimate to estimate each pixel value

Step 8: Repeat Steps 3-7 in the final estimate, considering the output of basic estimate as oracle in the final estimate and by replacing Hard thresholding with Wiener filtering.

Step 9: Calculate the Point Spread Function and number of iterations of the output from Step8.

Step 10: Apply R_L algorithm to denoise the outputs obtained from Step 9.

To estimate the quality of the denoised images attained by the proposed adaptive algorithm, five classes of standard image quality measure have been used: Peak - Signal - to - Noise - Ratio, Contrast - to - Noise - Ratio, Root - Mean - Square - Error, Bhattacharya-Coefficient and Edge-Preservation-Index at various Standard Deviation Values (2, 5, 10, 15, 20, 25, 30, 35, 40, 70, 50, and 100).

4. Comparative Parameters

4.1 Peak - Signal - to - Noise - Ratio

The Peak - Signal - to - Noise - Ratio articulates the ratio between the peak signal power that is achievable and the altering power of noise. PSNR in general is expressed as logarithmic scale due to the broad range as expressed in equation (14).

$$\text{PSNR} = 10 \log \left(\frac{M^2}{\text{MSE}} \right) \quad (14)$$

where M indicates the image maximum-pixel value that can diverge up to $2^{\text{bits}} - 1$, where bits= number of bits per sample. Peak - Signal - to - Noise - Ratio is an error-sensitivity metric that relies on the Mean-Square-Error value along with the image dynamic range.

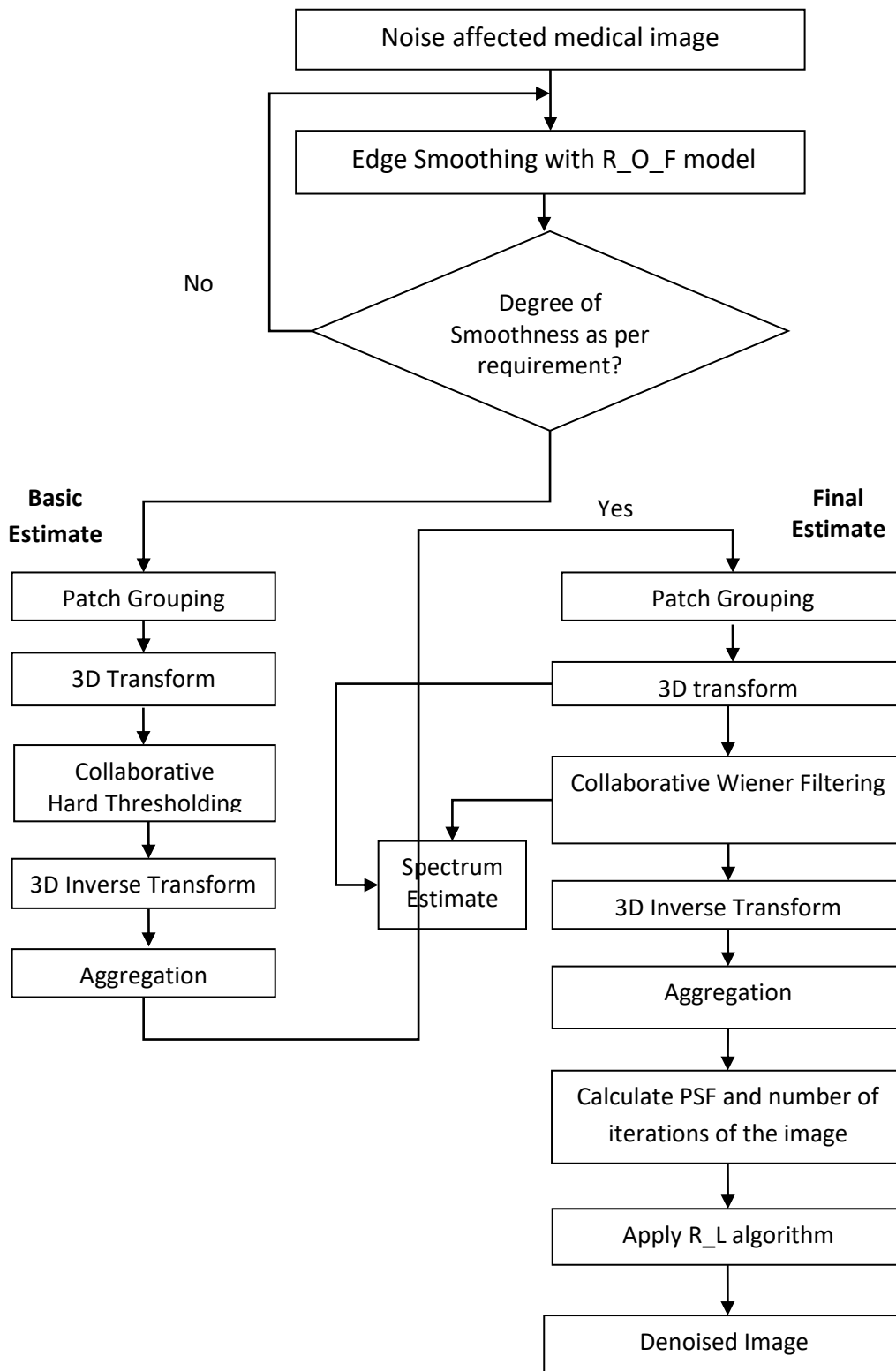


Fig.1. Flowchart of the proposed hybrid algorithm

4.2 Root - Mean - Square - Error

Root - Mean - Square - Error (R-MSE) indicated in equation (15) is the section value of standard deviation for various diversities along with experimental as well as expected values called as residuals. R-MSE evaluates the accuracy to identify errors generated by various models for a meticulous-data.

$$R - MSE(\hat{\theta}) = \sqrt{MSD(\hat{\theta})} = \sqrt{E(\hat{\theta} - \theta)^2} \quad (15)$$

Where $\hat{\theta}$ represents the estimator of an estimated parameter θ .

4.3 Contrast - to - Noise - Ratio

Contrast - to - Noise - Ratio (C - NR) expressed in equation (16) describes the image quality-metric, which is analogous to Signal-to-noise ratio but it subtracts a term before taking a ratio.

$$C - NR = \frac{|S_A - S_B|}{\sigma_0} \quad (16)$$

where S_A and S_B are the signal intensities formed in the region A and region B correspondingly, and σ_0 signifies the standard deviation of the Bhattacharya Coefficient noise present in an image.

4.4 Bhattacharya-Coefficient

Bhattacharya-Coefficient (BC) assess the relative proximity among two diverse probability-distributions x as well as y over a domain D , i.e., $D \in [0,255]$ for an 8-bit data as indicated in equation (17).

$$BC(x, y) = \sum_{p \in D} \sqrt{x(p)y(p)} \quad (17)$$

Bhattacharya-Coefficient evaluates the closeness amid two various discrete probability-distributions p and q over same domain X (for example, $X \in [0,255]$ for the 8-bit accurate data).

4.5 Edge-Preservation-Index

Edge-Preservation-Index (EPI) assesses the ability to preserve image details. Laplacian-kernel is utilized to generate the image binary-edge maps by detecting the weak edges. The mathematical computation of EPI is as represented in equation (18)

$$EPI = \frac{E(\Delta r - \overline{\Delta r}, \widehat{\Delta r} - \overline{\widehat{\Delta r}})}{\sqrt{E(\Delta r - \overline{\Delta r}, \overline{\Delta r} - \overline{\Delta r}) \cdot E(\widehat{\Delta r} - \overline{\widehat{\Delta r}}, \overline{\widehat{\Delta r}} - \overline{\widehat{\Delta r}})}} \quad (18)$$

Where $E(r_1, r_2)$ as shown in equation (19)

$$E(r_1, r_2) = \sum_{i,j \in R} r_1(i, j) \cdot r_2(i, j) \quad (19)$$

where $\Delta r(i, j)$ and $\widehat{\Delta r}(i, j)$ represents the high-pass-filter Region-of-Interest (R) in the reference of $r(i, j)$. $\overline{\Delta r}$ and $\overline{\widehat{\Delta r}}$ are the Region-of-Interest means of Laplacian filter.

5. Results and Discussion

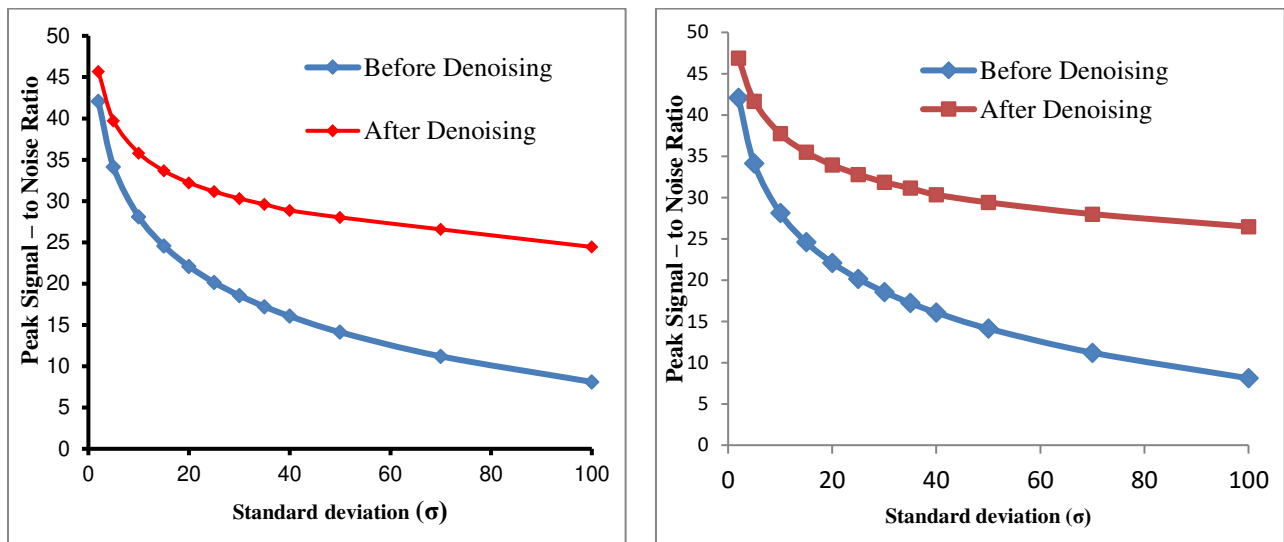
In this section, the experimentation and results obtained are detailed. In addition, relative performance of the proposed model is compared with the existing methodologies.

5.1. Experimentation

In this segment the results acquired with the help of the proposed adaptive method are presented and evaluated for its performance and are compared with the existing methodologies The proposed algorithms are implemented in the MATLAB platform. Two open-accesses datasets

containing chest X-ray images [62] and MRI/CT cancer images [64] are considered to evaluate the denoising performance of proposed adaptive method. From the first dataset a total of 500 chest X-ray images are considered randomly and resized to obtain uniform data. From the second dataset 400 slices of MRI and 350 slices of CT DICOM (Digital-Imaging and Communications in medicine) format images are considered. For implementation, at first, all the input images from datasets are corrupted by Gaussian noise at various standard deviations (2, 5, 10, 15, 20, 25, 30, 35, 50, 70, and 100). All these corrupted images are denoised by the proposed hybrid algorithm and the performance of the proposed algorithm is tested using various statistical parameters like PSNR, C-NR, R-MSE, BC and EPI.

Peak - Signal - to - Noise Ratio: The output image quality increases with the increase in the value of PSNR. Generally, the PSNR of the lossy image varies from 30 dB to 50 dB when a pixel is represented with 8 bits per sample. Fig 2 represents the variation of PSNR value with the change of standard deviation value of noise from 2 dB to 100 dB for chest X-Ray and MRI/CT datasets respectively. The value of PSNR is decreasing with the raise in the level of noise. The proposed adaptive method achieves a PSNR value of 47.44 dB for chest X-Ray dataset, and 46.86 dB for MRI/CT dataset at a standard deviation value of $\sigma = 2$ dB. PSNR value decreases to a value of 28.45 dB for chest X-Ray and 26.46 dB for MRI/CT dataset at a standard deviation value of $\sigma = 100$ dB respectively.



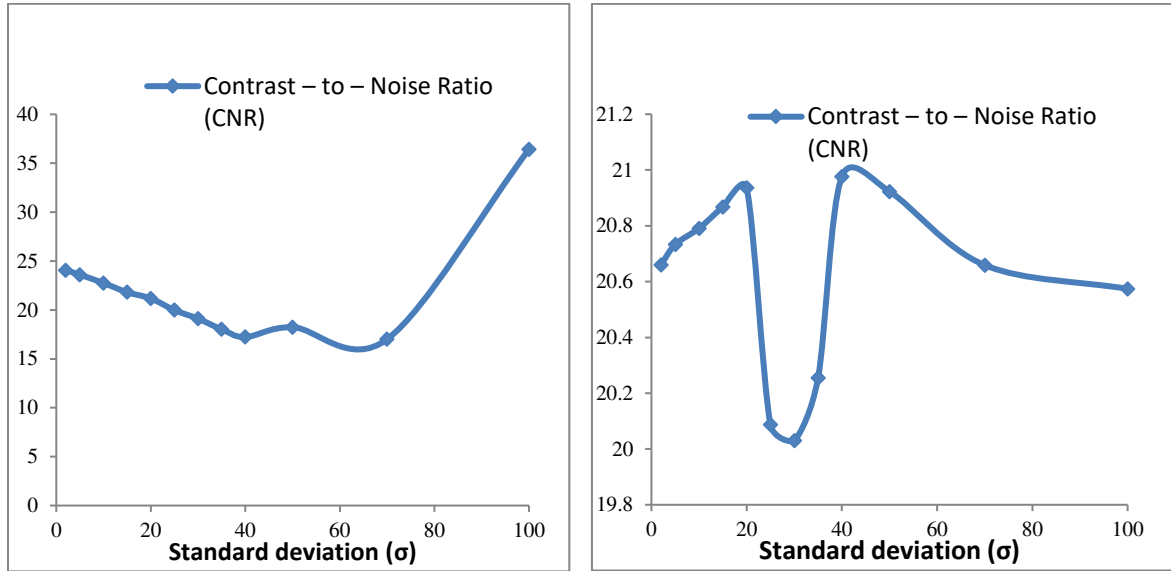
(a) Chest X-Ray Dataset

(b) MRI/CT Dataset

Fig.2. Peak - Signal - to - Noise Ratio (PSNR) at various Standard Deviations

Contrast - to - Noise Ratio (CNR): CNR access the probability of detecting lesion in medical images. CNR is a positive value that ranges from a value of '1' and ' ∞ '. As the value of CNR increases, the objects can be more easily visualized in the background. Fig 3 shows the variation of CNR with respect to the change of standard deviation of noise from 2 dB to 100 dB for chest

X-Ray and MRI/CT datasets respectively. The proposed adaptive method achieves a CNR value of 24.06 dB for chest X-Ray dataset and 20.660 dB for MRI/CT dataset at a standard deviation value of $\sigma = 2$ dB. CNR value varies to a value 36.43 dB for chest X-Ray and 20.574 dB for MRI/CT dataset at a standard deviation value of $\sigma = 100$ dB respectively.

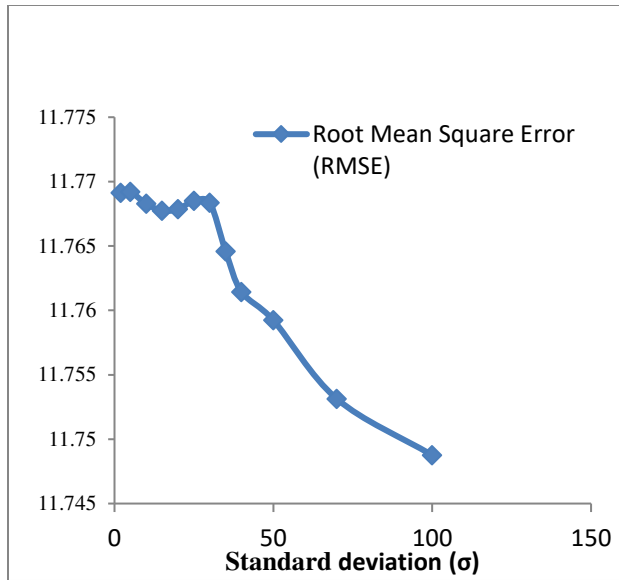


(a) Chest X-Ray Dataset

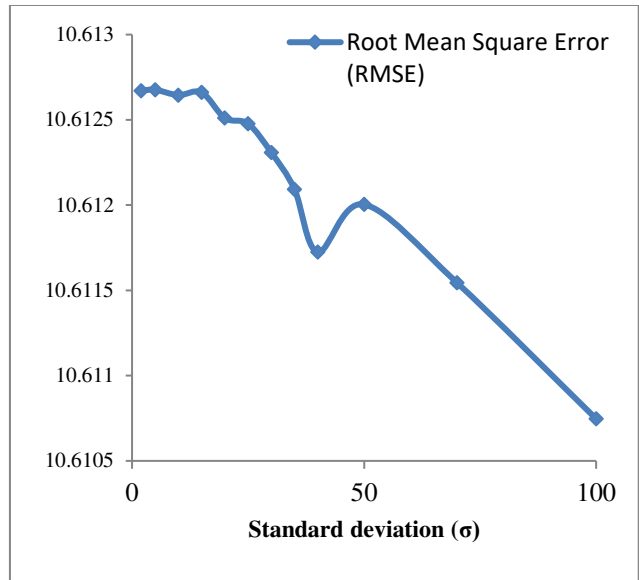
(b) MRI/CT Dataset

Fig.3. Contrast - to - Noise Ratio (CNR) at various Standard Deviations

Root Mean Square Error (RMSE): The quality of output is high when the lossy image has low value of RMSE. A relatively low RMSE value indicates the accuracy of the model. A perfect fit to data achieves a value of '0' RMSE. As the amount of noise increases the value of RMSE also increases resulting in loss of data. Fig 4 represents the variation of RMSE value with the change of standard deviation value of noise from 2 dB to 100 dB for chest X-Ray and MRI/CT datasets respectively. The proposed adaptive method achieves a RMSE value of 10.651732 dB for chest X-Ray dataset and 10.655123 dB for MRI/CT dataset at a standard deviation value of $\sigma = 2$ dB respectively. RMSE value changes to a value 11.769128 dB for chest X-Ray and 11.748757 dB for MRI/CT dataset at a standard deviation value of $\sigma = 100$ dB respectively.



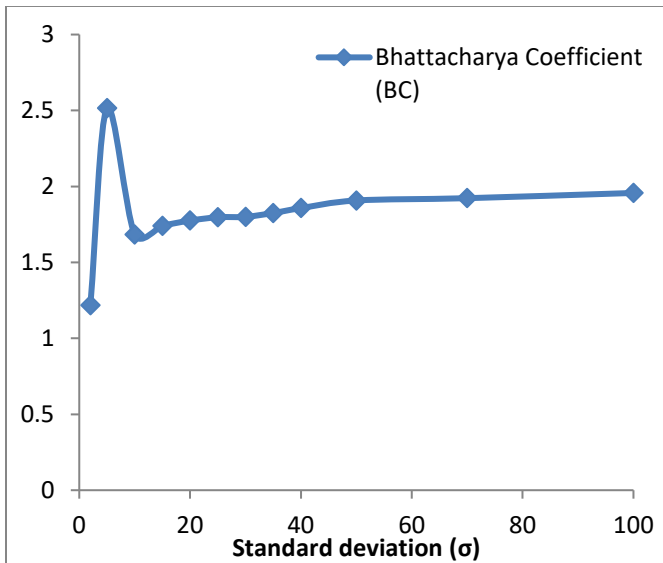
(a) Chest X-Ray Dataset



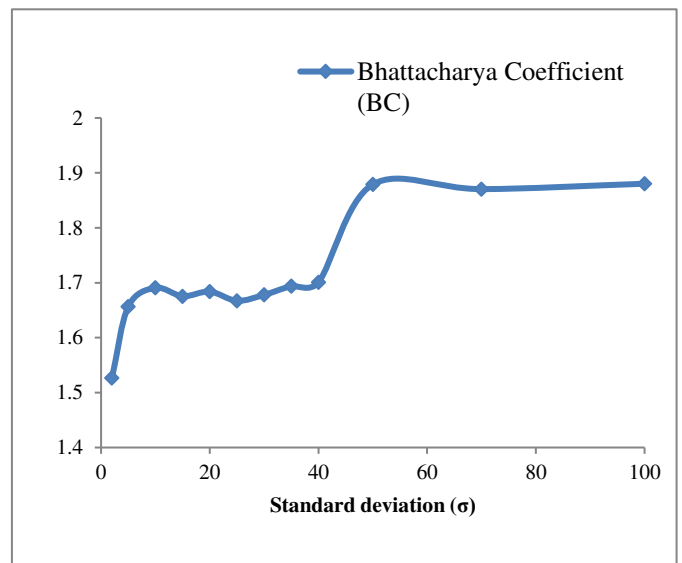
(b) MRI/CT Dataset

Fig.4. Root Mean Square Error (RMSE) at various Standard Deviations

Bhattacharya Coefficient (BC): The quality of output is high when the lossy image has low value of BC. A perfect match between two distributions results in a value of BC as ‘0’. As the amount of overlap increases, the value of BC also increases. Fig 5 represents the variation of BC value with the change of standard deviation value of noise from 2 dB to 100 dB for chest X-Ray and MRI/CT datasets. The proposed adaptive method achieves a BC value of 1.6610 dB for chest X-Ray dataset and 2.5017 dB for MRI/CT dataset at a standard deviation value of $\sigma = 2$ dB. BC value changes to a value 1.5266 dB for chest X-Ray and 1.8802 dB for MRI/CT dataset at a standard deviation value of $\sigma = 100$ dB respectively.



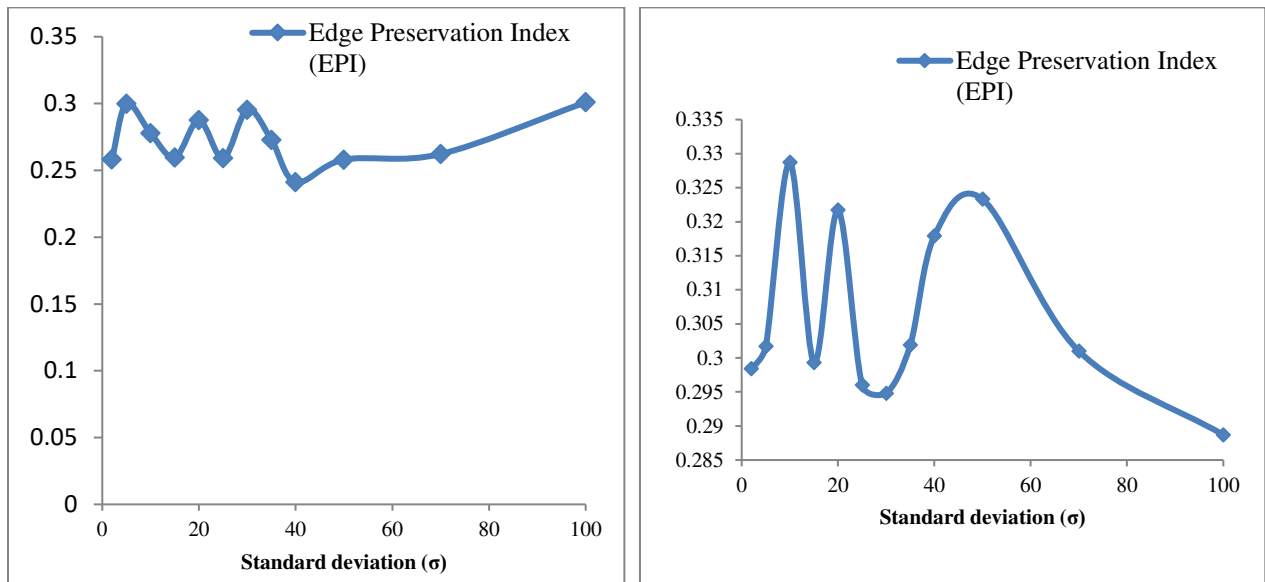
(a) Chest X-Ray Dataset



(b) MRI/CT Dataset

Fig.5. Bhattacharya Coefficient (BC) various Standard Deviations

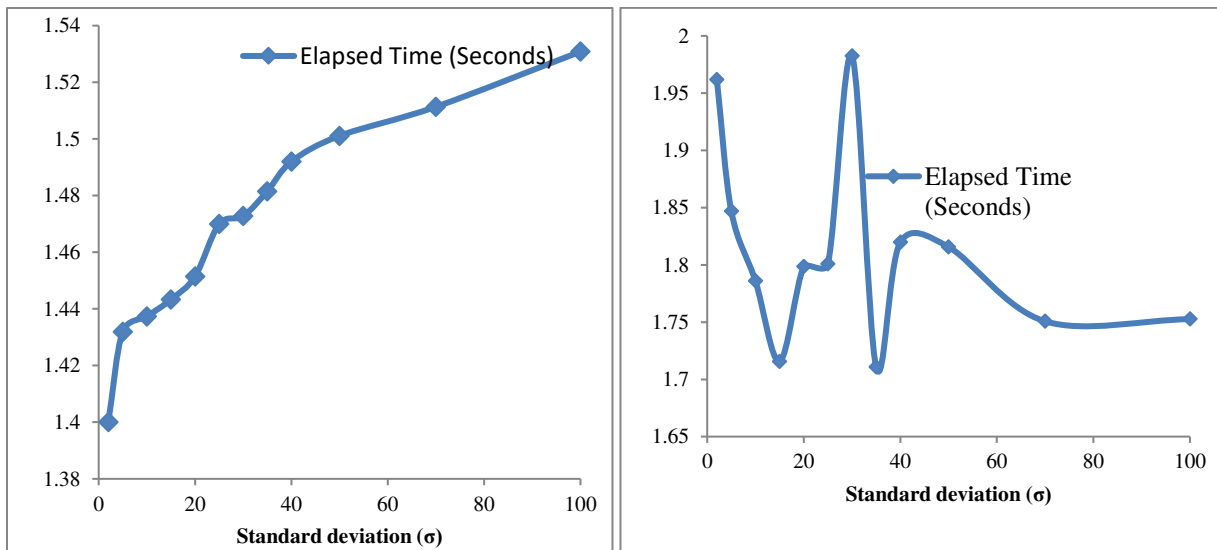
Edge Preservation Index (EPI): The EPI is a positive value that ranges between ‘0’ and ‘1’. If the value of EPI is closer to ‘1’, then the edge is well preserved. As the levels of noise increases, the value of EP linearly decreases. Fig 6 represents the variation of BC value with the change of standard deviation of noise from 2 dB to 100 dB for chest X-Ray and MRI/CT datasets. The proposed adaptive method achieves a BC value of 0.4398 dB for chest X-Ray dataset and 0.5030 dB for MRI/CT dataset at a standard deviation value of $\sigma = 2$ dB. BC value changes to a value 0.2984 dB for chest X-Ray and 0.2887 dB for MRI/CT dataset at a standard deviation value of $\sigma = 100$ dB respectively.



(a) Chest X-Ray Dataset

(b) MRI/CT Dataset

Fig.6. Edge Preservation Index (EPI) at various Standard Deviations



(a) Chest X-Ray Dataset**(b) MRI/CT Dataset****Fig.7. Elapsed Time (Seconds) of MRI Image at various Standard Deviations**

Table 1 and Table 2 present the quantitative outcomes of the proposed system for chest X-ray dataset and MRI/CT dataset using various statistical parameters at different standard deviations (σ) respectively.

Table 1. Average Statistical parameters for Chest X-Ray image dataset

Standard deviation (σ)	Peak Signal – to Noise Ratio (PSNR)		Contrast – to – Noise Ratio (CNR)	Root Mean Square Error (RMSE)	Bhattacharya Coefficient (BC)	Edge Preservation Index (EPI)	Elapsed Time (Seconds)
	Before Denoising	After Denoising					
2	42.088	47.4433	24.06	10.651732	1.6610	0.4398	2.235768
5	34.129	42.9890	23.60	10.651765	2.0139	0.4824	2.369741
10	28.108	39.8848	22.75	10.652133	2.1445	0.4973	2.115846
15	24.586	37.9942	21.81	10.652524	2.1832	0.4773	2.371193
20	22.088	36.5408	21.17	10.653165	2.2148	0.4495	2.368134
25	20.149	35.4237	19.98	10.653873	2.2798	0.4246	2.196733
30	18.566	34.4751	19.10	10.653101	2.3033	0.4648	2.353988
35	17.277	33.6664	18.02	10.654884	2.3168	0.4085	2.270163
40	16.067	32.9897	17.23	10.653038	2.3806	0.4356	2.251937
50	14.129	32.0585	18.24	10.654638	2.3903	0.4211	2.250507
70	11.206	30.3681	17.01	10.653887	2.4379	0.4665	2.364166
100	8.108	28.4598	36.43	10.655123	2.5017	0.5030	2.179279


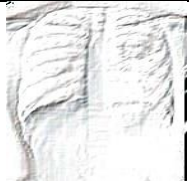
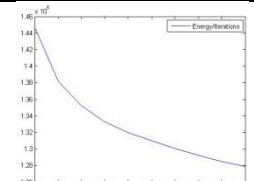



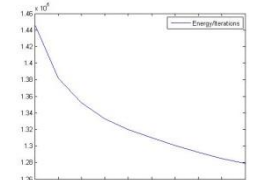


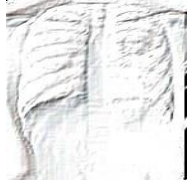
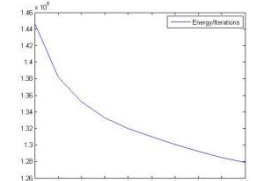


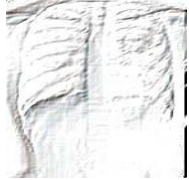
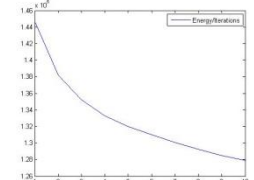


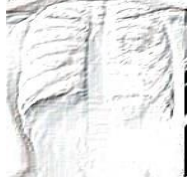
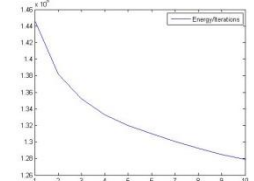


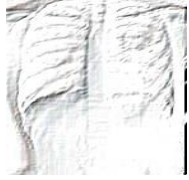
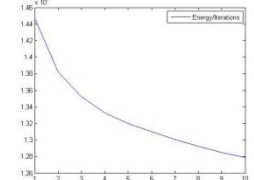



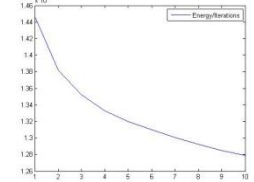

Table 3 and Table 4 shows the quantitative outcomes of the proposed system displaying the images of the noisy chest X-ray dataset and MRI/CT dataset, edge detected images, energy per iterations and denoised images at various σ values respectively. Figures (2-7) represent the comparison of various performance metrics at various σ values.

Table 2. Average Statistical parameters for MRI/CT image dataset

Standard deviation (σ)	Peak Signal – to Noise Ratio (PSNR)		Contrast – to – Noise Ratio (CNR)	Root Mean Square Error (RMSE)	Bhattacharya Coefficient (BC)	Edge Preservation Index (EPI)	Elapsed Time (Seconds)
	Before Denoising	After Denoising					
2	42.083	46.8674	20.660	11.769128	1.5266	0.2984	1.961876
5	34.124	41.6632	20.733	11.769207	1.6566	0.3017	1.846779
10	28.104	37.7228	20.791	11.768276	1.6907	0.3287	1.785858
15	24.582	35.4842	20.868	11.767747	1.6755	0.2993	1.715549
20	22.083	33.9441	20.936	11.767856	1.6838	0.3217	1.798439
25	20.145	32.7913	20.087	11.768507	1.6671	0.2960	1.800863
30	18.561	31.8603	20.030	11.768359	1.6779	0.2948	1.982480
35	17.222	31.1270	20.255	11.764582	1.6938	0.3019	1.710677
40	16.062	30.3427	20.977	11.761428	1.7009	0.3179	1.819741
50	14.124	29.4090	20.923	11.759235	1.8789	0.3233	1.815613

70	11.202	27.9855	20.659	11.753124	1.8704	0.3010	1.750690
100	8.104	26.4645	20.574	11.748757	1.8802	0.2887	1.752613

Table.3. Qualitative Results of Chest X-Ray image dataset at various Standard Deviations

Standard deviation (σ)	Noisy Image	Edge Detection	Energy per Iterations	Denosed Image
2				
5				
10				
15				
20				
25				
30				


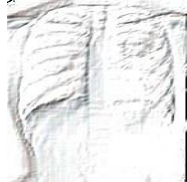
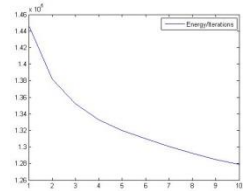


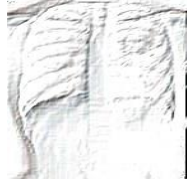
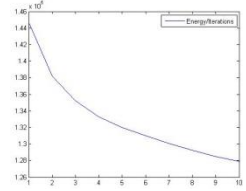


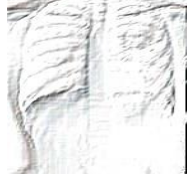
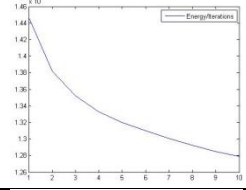


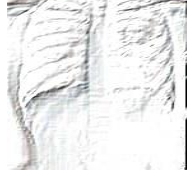
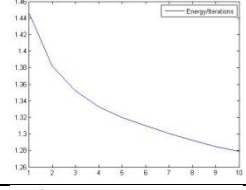


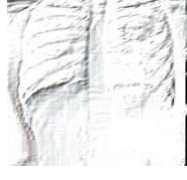
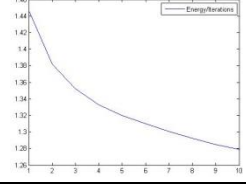


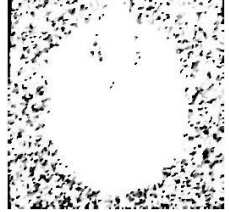
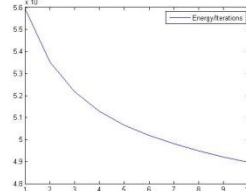


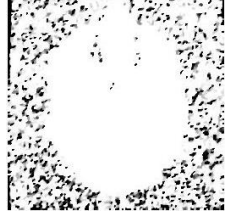
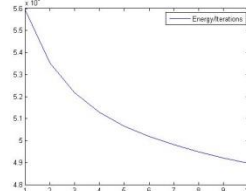



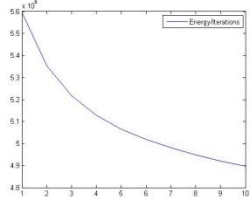



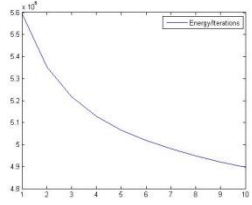

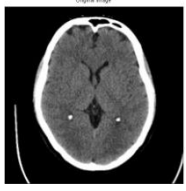
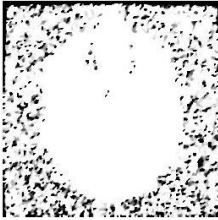
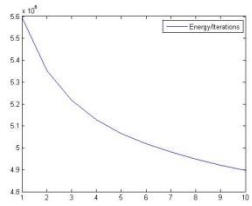
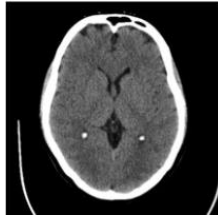
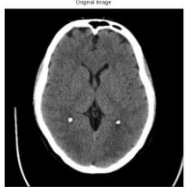
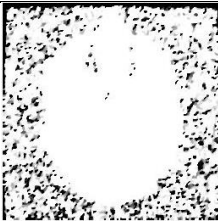
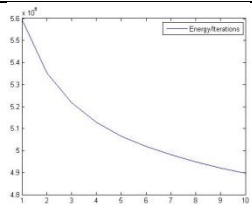
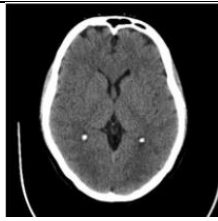
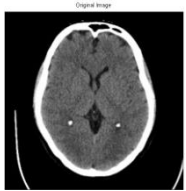
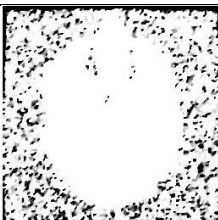
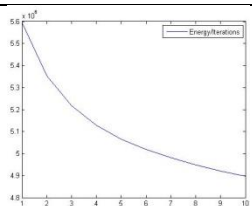


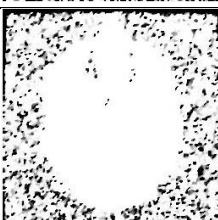
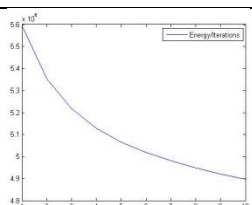

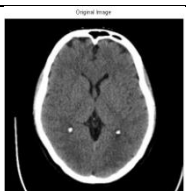
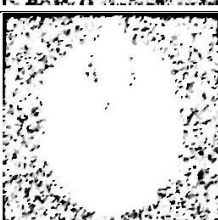
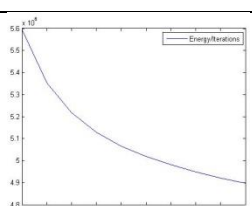
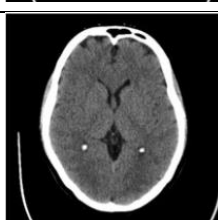
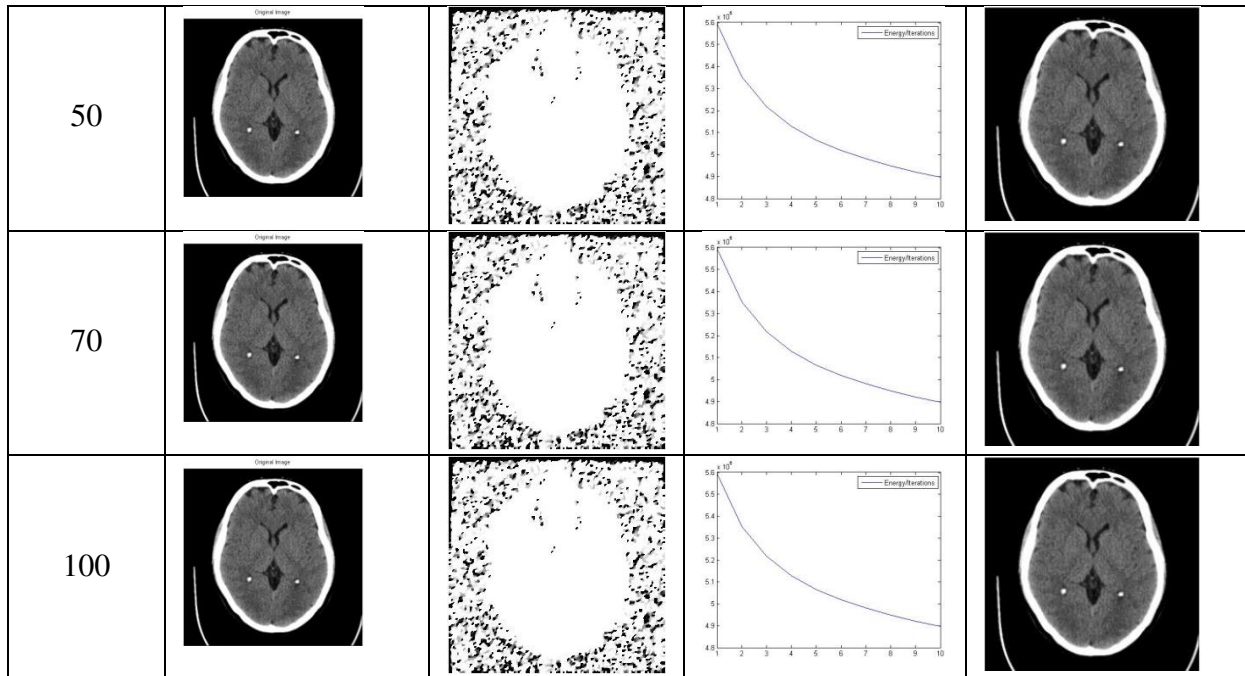
35				
40				
50				
70				
100				

Table.4. Qualitative Results of MRI/CT image dataset at various Standard Deviations

Standard deviation (σ)	Noisy Image	Edge Detection	Energy per Iterations	Denoised Image
2				
5				

10				
15				
20				
25				
30				
35				
40				



The average PSNR value of proposed approach for both the datasets are recorded in Table 5 and compared with the existing methods. This shows that the adaptive technique proposed achieves high PSNR value of 47.44 dB for Chest X-ray images and 46.86 dB for MRI/CT images compared to the previous approaches. Table 6 represents the comparison of the R-MSE values of the proposed approach with the previous approaches. The proposed approach attains a value of 10.65 dB and 11.76 dB for chest X-ray and MRI/CT images respectively. By comparing the approaches, a conclusion can be drawn that the proposed approach results in minimum error value compared to the previous approaches. Table 7 represents the comparison of the proposed approach with the existing methods using C-NR value. The proposed scheme attains a high C-NR value of 24.06 dB and 20.66 dB for chest X-ray and MRI/CT images respectively compared to the earlier approaches. From the computed numerical values of the statistical parameters, it is concluded that the adaptive methodology proposed effectively removes the noise without loss of the useful information of the medical image.

Table.5. Comparison of medical image denoising techniques with respect to PSNR

Denoising Technique	PSNR (dB)	Dataset	Noise	Limitations
Linear_filter [66]	20.07	Cyst dataset	Gaussian	Blurs the image edges
Anisotropic_Diffusion [67]	25.3	1. T2 3-D MRI volume 2. 3-D SPOiled Gradient Recalled MR	Rician	Applicable only for Gaussian assumption

		data set		
Fourth-order_Partial-Differential Equation [68]	17.20	MRI data by Siemens Vision 1.5 Tesla MR scanner	Gaussian	Results in the unavoidable speckles
Non-Local Means [69]	34.42	MRI images of the brain	Fractional Brownian motion noise	Increases computational complexity due to the quadratic nature of pixels
Bilateral filter [70]	20.77	BrainWeb image data of T1-weighted 1mm and 5mm MR image volumes	Gaussian	Time consuming and monotonic process
Trilateral filter [71]	26.70	2D and 3D biomedical datasets, 3D-numerical phantoms, 3D MRI phantom	Additive White Gaussian	Loss of sparsity
Wavelet Transform [72]	22.31	Gray-Scale MRI images	Rician, Gaussian, Salt & pepper	High number of coefficients
Wavelet Shrinkage [73]	37.32	MRI images	Gaussian	Does not deal with local smoothness
Curvelet transform [74]	27.40	MRI images	White noise	Leads to curve shaped artifacts
Contourlet transform [75]	25.88	MRI slicing Image	Gaussian	high computational complexity
BM3D-NIDe-VST [76]	31.86	Alzheimer's Disease Neuroimaging Initiatedatabase	Gaussian	efficiently works in homogeneous regions only
Anisotropic_Diffusion + Laplacian Kernel [77]	26.28	MRI images	Random noise	High computational time
Deep CNN [78]	23.88	MRI images	Gaussian	efficient in homogeneous regions only
Maximum Likelihood Estimation [79]	36.02	MRI images	Rician	Leads to tradeoff when the system is affected by Rician noise
Linear_Mean-Square Error Estimation [80]	41.06	MRI images	Rician	3D MR data redundancy cannot be considered as advantage
Non-Local_Maximum Likelihood Estimation [81]	34.28	MRI images	Gaussian	less adaptive
Block-Matching_4-Dimensional Filtering [82]	40.38	MRI images	Gaussian	less adaptive to unpredictable image contents

MR-image denoising with the help of Kolmogorov_Smirnov distance [83]	28.7	MRI images	Gaussian	extremely sensitive to the noise deviations
Chi-Square Unbiased Risk Estimation [84]	21.55	MRI images	Gaussian	Lack of sparsity and hence is limited to small sample size
Adaptive_Decision Based Median Filter [85]	35.12	Medical Images	Gaussian	Only used in complex domain
Local-Polynomial based Intersection-Confidence_Interval Filter + Genetic-Algorithm [86]	19.59	MRI brain images	Rician noise	Leads to stripe artifacts at homogeneous regions
Complex-Valued Convolutional Neural Network-Based Model [63]	37.20	chest X-ray images	additive white Gaussian noise	may be tried out for better compactness and generalizability
Unsupervised Deep Learning Approach [65]	42.74	MRI/CT images	Poisson	Have to overcome any degradation in the medical imagery along with the noise
Proposed Adaptive Algorithm – Chest X-Ray Dataset	47.44			
Proposed Adaptive Algorithm – MRI/CT Dataset	46.86			

Table.6. Comparison of various medical-image denoising techniques with respect to R-MSE

Denoising Technique	R-MSE	Dataset	Noise	Limitations
Wavelet based denoising of image [87]	14.3454	Gray-Scale MRI images	Rician, Gaussian, Salt & pepper	High number of coefficients
Filtering based denoising of image [88]	11.4815	ultrasound medical images	Poisson noise, amplifier noise, Salt and Pepper Noise, Speckle Noise	Time consuming and monotonic process
Optimal bilateral filter and convolutional neural network [89]	11.25	MRI and CT medical images	Rician	Limited to small sample sizes
Fuzzy Based Denoising [90]	14.9663	medical	Poisson	Computationally

		images		complex
Non-Local Means [91]	10.83	MRI images of the brain	Fractional Brownian motion noise	enhance computational complexity due to the pixels quadratic nature
Multi-stage Directional Median Filtering [92]	22.75	MRI images	Gaussian	High time requirement
Gaussian Filtering [93]	21.56	Gray-Scale MRI images	Rician, Gaussian, Salt & pepper	Blurs the image edges
Entropy paramounted linear regression filter [94]	8.256	normal heart Apical four chamber view image	speckle noise	less adaptive to variable image contents
Unsupervised Deep Learning Approach [65]	16.557	MRI/CT images	Poisson	Have to overcome any degradation in the medical imagery along with the noise
Proposed Adaptive Algorithm – Chest X-Ray Dataset	10.65			
Proposed Adaptive Algorithm – MRI/CT Dataset	11.76			

Table.7. Comparison of various medical-image denoising methods with respect to C-NR

Denoising Technique	CNR (dB)	Dataset	Noise	Limitations
Deep convolutional neural networks [95]	11.71	3D brain phantom from BrainWeb	statistical image noise	may be tried out for better compactness and generalizability
BM3D [96]	7.73	X-ray microtomography	Gaussian	Loss of Sparsity
Context-based BM3D [97]	2.48	low-dose CT images	Gaussian	Does not deal with local smoothness
Two-dimensional Curvelet-based dictionary learning [98]	5.12	100 publically available OCT B-scans with and	speckle noise	Leads to curve shaped artifacts

		without non-neovascular age-related macular degeneration (AMD)		
Deep learning image reconstruction [99]	11.58	portal venous phase abdominal CT	Gaussian	efficient in homogeneous regions only
Proposed Adaptive Algorithm – Chest X-Ray Dataset	24.06			
Proposed Adaptive Algorithm – MRI/CT Dataset	20.66			

6. Conclusion and Future scope

A novel hybrid adaptive approach using Block Matching, Richardson_Lucy (R_L) Algorithm, Rudin_Osher_Fatemi (R_O_F) preprocessing is proposed in this paper for medical image denoising. While R_O_F model is used to detect the edges of the medical image, BM3D and R_L algorithms are utilized to denoise the medical images. Two realistic datasets, one on chest X-ray and another on MRI/CT are considered and simulated to evaluate the performance indices at various noise intensities. The performance of the proposed adaptive technique is compared with the state-of-the-art denoising methods in terms of various statistical parameters of PSNR, CNR, RMSE, BC and EPI. It is observed that the proposed methodology outperforms all the existing methods with a considerable margin at all the noise levels. From the quantitative and qualitative performance analysis, it is observed that the proposed method reduced the noise and restored the images more effectively than the existing methods. Further this approach can be improvised in future by extending the approaches to the video frameworks for live images in the medical fields.

Conflict of interest statement: The authors declare that they have no known competing financial interests or personal relationships that could have appeared to influence the work reported in this paper.

Role of funding source: Not Applicable

Ethical Approval: This article does not contain any studies with human participants or animals performed by any of the authors.

Informed Consent [if applicable]: Not Applicable.

Authors' Contribution: Ambika Annavarapu, Surekha Borra contributed methodology and paper writing; Vijay Bhaskar Reddy Dinnepu contributed Data collection; Mankamana Prasad Mishra contributed Data analysis and review.

References

1. Dey, N., Ashour, A. S., Shi, F., & Balas, V. E. (2018). *Soft Computing Based Medical Image Analysis*. Academic Press.
2. Chaki, J., & Dey, N. (2018). *A beginner's guide to image preprocessing techniques*. CRC Press.
3. Baselice, F., Ferraioli, G., Ambrosanio, M., Pascazio, V., & Schirinzi, G. (2018). Enhanced Wiener filter for ultrasound image restoration. *Computer methods and programs in biomedicine*, 153, 71-81.
4. Ali, H. M. (2018). MRI medical image denoising by fundamental filters. In *High-Resolution Neuroimaging-Basic Physical Principles and Clinical Applications*. InTech.
5. You, Y. L., & Kaveh, M. (2000). Fourth-order partial differential equations for noise removal. *IEEE Transactions on Image Processing*, 9(10), 1723-1730
6. Buades, A., Coll, B., & Morel, J. M. (2005). A review of image denoising algorithms, with a new one. *Multiscale Modeling & Simulation*, 4(2), 490-530.
7. Agrawal, S., & Sahu, R. (2012). Wavelet based MRI image denoising using thresholding techniques. *International Journal of Science, Engineering and Technology Research (IJSETR) Volume, 1*.
8. Starck, J. L., Candès, E. J., & Donoho, D. L. (2002). The Curvelet transform for image denoising. *IEEE Transactions on image processing*, 11(6), 670-684.
9. JannathFirthouse.P, ShajunNisha.S and Dr.M.MohammedSathik, “Noise Reduction in MRI Images using Contourlet Transform and Threshold Shrinkages Techniques”, *International Journal of Computer Science and Information Technologies*, Vol. 7 (2) , 2016, 723-728
10. Kaur, S., Chaudhary, G., Dinesh Kumar, J., Pillai, M. S., Gupta, Y., Khari, M., et al. (InPress). Optimizing Fast Fourier Transform (FFT) Image Compression using Intelligent Water Drop (IWD) Algorithm. *International Journal Of Interactive Multimedia And Artificial Intelligence*, In Press(In Press), 1-8. <http://doi.org/10.9781/ijimai.2022.01.004>
11. David H. Ackley, Geoffrey E. Hinton, and Terrence J. Sejnowski. A learning algorithm for Boltzmann machines. *Cognitive Science*, 9:147–169, 1985.

12. Jain, V., & Seung, S. (2009). Natural image denoising with convolutional networks. In *Advances in Neural Information Processing Systems* (pp. 769-776).
13. Gondara, L. (2016, December). Medical image denoising using convolutional denoising Autoencoders. In *Data Mining Workshops (ICDMW), 2016 IEEE 16th International Conference on* (pp. 241-246). IEEE
14. Misra, Debajyoti, et al. "Effect of using genetic algorithm to denoise MRI images corrupted with Rician Noise." *Emerging Trends in Computing, Communication and Nanotechnology (ICE-CCN), 2013 International Conference on*. IEEE, 2013.
15. Dey, N., Chaki, J., Moraru, L., Fong, S., & Yang, X. S. (2020). Firefly algorithm and its variants in digital image processing: A comprehensive review. *Applications of firefly algorithm and its variants*, 1-28.
16. Chakraborty, S., Chatterjee, S., Ashour, A. S., Mali, K., & Dey, N. (2018). Intelligent computing in medical imaging: a study. In *Advancements in applied metaheuristic computing* (pp. 143-163). IGI global.
17. Diaz, M., Crispo, G., Parziale, A., Marcelli, A., & Ferrer, M. A. (InPress). Writing Order Recovery in Complex and Long Static Handwriting. *International Journal Of Interactive Multimedia And Artificial Intelligence*, In Press(In Press), 1-14. <http://doi.org/10.9781/ijimai.2021.04.003>
18. Khattak, M. I., Al-Hasan, M. 'ath, Jan, A., Saleem, N., Verdú, E., & Khurshid, N. (2021). Automated Detection of COVID-19 using Chest X-Ray Images and CT Scans through Multilayer- Spatial Convolutional Neural Networks. *International Journal Of Interactive Multimedia And Artificial Intelligence*, 6(Regular Issue), 15-24. <http://doi.org/10.9781/ijimai.2021.04.002>
19. Khattak, M. I., Al-Hasan, M. 'ath, Jan, A., Saleem, N., Verdú, E., & Khurshid, N. (2021). Automated Detection of COVID-19 using Chest X-Ray Images and CT Scans through Multilayer- Spatial Convolutional Neural Networks. *International Journal Of Interactive Multimedia And Artificial Intelligence*, 6(Regular Issue), 15-24. <http://doi.org/10.9781/ijimai.2021.04.002>
20. Pour, NavidSaffari, and Amir Hossein Javanshir. "A robust approach for medical image denoising using fuzzy clustering." *INTERNATIONAL JOURNAL OF COMPUTER SCIENCE AND NETWORK SECURITY* 17.6 (2017): 241-247.

21. Ashour, A. S., Beagum, S., Dey, N., Ashour, A. S., Pistolla, D. S., Nguyen, G. N., ... & Shi, F. (2018). Light microscopy image de-noising using optimized LPA-ICI filter. *Neural Computing and Applications*, 29(12), 1517-1533.
22. Rajan, Jeny&Jeurissen, Ben &Verhoye, Marleen &Audekerke, Johan &Sijbers, Jan. (2011). Maximum likelihood estimation-based denoising of magnetic resonance images using restricted local neighborhoods. *Physics in medicine and biology*. 56. 5221-34. 10.1088/0031-9155/56/16/009.
23. Luo, Jianhua, et al. "Magnetic resonance image denoising using spectral data substitution." *Image and Signal Processing (CISP), 2010 3rd International Congress on*. Vol. 2. IEEE, 2010.
24. Awate, Suyash P., and Ross T. Whitaker. "Nonparametric neighborhood statistics for MRI denoising." *Biennial International Conference on Information Processing in Medical Imaging*. Springer, Berlin, Heidelberg, 2005.
25. Sudeep, P. V., et al. "Nonlocal linear minimum mean square error methods for denoising MRI." *Biomedical Signal Processing and Control* 20 (2015): 125-134.
26. He, L., & Greenshields, I. R. (2008). A nonlocal maximum likelihood estimation method for Rician noise reduction in MR images. *IEEE transactions on medical imaging*, 28(2), 165-172.
27. Dabov, K., Foi, A., Katkovnik, V., & Egiazarian, K. (2006, February). Image denoising with block-matching and 3D filtering. In *Image Processing: Algorithms and Systems, Neural Networks, and Machine Learning* (Vol. 6064, p. 606414). International Society for Optics and Photonics.
28. Dabov, K., Foi, A., Katkovnik, V., & Egiazarian, K. (2007). Image denoising by sparse 3-D transform-domain collaborative filtering. *IEEE Transactions on image processing*, 16(8), 2080-2095.
29. Dabov, K., Foi, A., Katkovnik, V., & Egiazarian, K. (2009, April). BM3D image denoising with shape-adaptive principal component analysis. In *SPARS'09-Signal Processing with Adaptive Sparse Structured Representations*.
30. Chen, Q., & Wu, D. (2010). Image denoising by bounded block matching and 3D filtering. *Signal Processing*, 90(9), 2778-2783.

31. Lebrun, M. (2012). An analysis and implementation of the BM3D image denoising method. *Image Processing On Line*, 2, 175-213.
32. Burger, H. C., Schuler, C. J., & Harmeling, S. (2012, June). Image denoising: Can plain neural networks compete with BM3D?. In *2012 IEEE conference on computer vision and pattern recognition* (pp. 2392-2399). IEEE.
33. Zhong, H., Ma, K., & Zhou, Y. (2015). Modified BM3D algorithm for image denoising using nonlocal centralization prior. *Signal Processing*, 106, 342-347.
34. Sarjanoja, S., Boutellier, J., & Hannuksela, J. (2015, September). BM3D image denoising using heterogeneous computing platforms. In *2015 Conference on Design and Architectures for Signal and Image Processing (DASIP)* (pp. 1-8). IEEE.
35. Li, Y., Zhang, J., & Wang, M. (2017). Improved BM3D denoising method. *IET Image Processing*, 11(12), 1197-1204.
36. Hasan, M., & El-Sakka, M. R. (2018). Improved BM3D image denoising using SSIM-optimized Wiener filter. *EURASIP Journal on Image and Video Processing*, 2018(1), 1-12.
37. Mäkinen, Y., Azzari, L., & Foi, A. (2019, September). Exact transform-domain noise variance for collaborative filtering of stationary correlated noise. In *2019 IEEE International Conference on Image Processing (ICIP)* (pp. 185-189). IEEE.
38. Wang, H., Cao, S., Jiang, K., Wang, H., & Zhang, Q. (2019). Seismic data denoising for complex structure using BM3D and local similarity. *Journal of Applied Geophysics*, 170, 103759.
39. Zhao, T., Hoffman, J., McNitt-Gray, M., & Ruan, D. (2019). Ultra-low-dose CT image denoising using modified BM3D scheme tailored to data statistics. *Medical physics*, 46(1), 190-198.
40. Yahya, A. A., Tan, J., Su, B., Hu, M., Wang, Y., Liu, K., & Hadi, A. N. (2020). BM3D image denoising algorithm based on an adaptive filtering. *Multimedia Tools and Applications*, 79(27), 20391-20427.
41. Hanchate, V., & Joshi, K. (2020). MRI denoising using BM3D equipped with noise invalidation denoising technique and VST for improved contrast. *SN Applied Sciences*, 2(2), 1-8.

42. Esedoğlu, S., & Osher, S. J. (2004). Decomposition of images by the anisotropic Rudin-Osher-Fatemi model. *Communications on Pure and Applied Mathematics: A Journal Issued by the Courant Institute of Mathematical Sciences*, 57(12), 1609-1626.
43. Aubert, G., & Aujol, J. F. (2005). Modeling very oscillating signals. Application to image processing. *Applied Mathematics and Optimization*, 51(2), 163-182.
44. Haddad, A., & Meyer, Y. (2007). An improvement of Rudin–Osher–Fatemi model. *Applied and Computational Harmonic Analysis*, 22(3), 319-334.
45. Chambolle, A., Caselles, V., Cremers, D., Novaga, M., & Pock, T. (2010). An introduction to total variation for image analysis. *Theoretical foundations and numerical methods for sparse recovery*, 9(263-340), 227.
46. Getreuer, P. (2012). Rudin-Osher-Fatemi total variation denoising using split Bregman. *Image Processing On Line*, 2, 74-95.
47. Said, A. B., Hadjidj, R., & Fougou, S. (2019). Total Variation for Image Denoising Based on a Novel Smart Edge Detector: An Application to Medical Images. *Journal of Mathematical Imaging and Vision*, 61(1), 106-121.
48. Phan, T. D. K. (2020). A weighted total variation based image denoising model using mean curvature. *Optik*, 217, 164940.
49. Fish, D. A., Brinicombe, A. M., Pike, E. R., & Walker, J. G. (1995). Blind deconvolution by means of the Richardson–Lucy algorithm. *JOSA A*, 12(1), 58-65.
50. Dell'Acqua, F., Scifo, P., Rizzo, G., Catani, M., Simmons, A., Scotti, G., & Fazio, F. (2010). A modified damped Richardson–Lucy algorithm to reduce isotropic background effects in spherical deconvolution. *Neuroimage*, 49(2), 1446-1458.
51. Yongpan, W., Huajun, F., Zhihai, X., Qi, L., & Chaoyue, D. (2010). An improved Richardson–Lucy algorithm based on local prior. *Optics & Laser Technology*, 42(5), 845-849.
52. Tam, N. W., Lee, J. S., Hu, C. M., Liu, R. S., & Chen, J. C. (2011). A Haar-wavelet-based Lucy–Richardson algorithm for positron emission tomography image restoration. *Nuclear Instruments and Methods in Physics Research Section A: Accelerators, Spectrometers, Detectors and Associated Equipment*, 648, S122-S127.

53. Wu, J. L., Chang, C. F., & Chen, C. S. (2013). An adaptive Richardson-Lucy algorithm for single image deblurring using local extrema filtering. *Journal of applied science and engineering*, 16(3), 269-276.
54. Yang, H. L., Huang, P. H., & Lai, S. H. (2014). A novel gradient attenuation Richardson–Lucy algorithm for image motion deblurring. *Signal Processing*, 103, 399-414.
55. Chen, D., Xiao, H., & Xu, J. (2019). An improved Richardson-Lucy iterative algorithm for C-scan image restoration and inclusion size measurement. *Ultrasonics*, 91, 103-113.
56. Belarbi, M. A., Mahmoudi, S., & Belalem, G. (2017). PCA as dimensionality reduction for large-scale image retrieval systems. *International Journal of Ambient Computing and Intelligence (IJACI)*, 8(4), 45-58.
57. Yang, X., & Jiang, X. (2020). A hybrid active contour model based on new edge-stop functions for image segmentation. *International Journal of Ambient Computing and Intelligence (IJACI)*, 11(1), 87-98.
58. Chowdhury, L., Kamal, M. S., Ripon, S. H., Parvin, S., Hussain, O. K., Ashour, A., & Chowdhury, B. R. (2021). A Biological Data-Driven Mining Technique by Using Hybrid Classifiers With Rough Set. *International Journal of Ambient Computing and Intelligence (IJACI)*, 12(3), 123-139.
59. Tali, R. V., Borra, S., & Mahmud, M. (2021). Detection and Classification of Leukocytes in Blood Smear Images: State of the Art and Challenges. *International Journal of Ambient Computing and Intelligence (IJACI)*, 12(2), 111-139.
60. Sharma, K., & Virmani, J. (2017). A decision support system for classification of normal and medical renal disease using ultrasound images: a decision support system for medical renal diseases. *International Journal of Ambient Computing and Intelligence (IJACI)*, 8(2), 52-69.
61. Kermany, D. S., Goldbaum, M., Cai, W., Valentim, C. C., Liang, H., Baxter, S. L., ... & Zhang, K. (2018). Identifying medical diagnoses and treatable diseases by image-based deep learning. *Cell*, 172(5), 1122-1131.
62. Rawat, Shubhankar, K. P. S. Rana, and Vineet Kumar. "A novel complex-valued convolutional neural network for medical image denoising." *Biomedical Signal Processing and Control* 69 (2021): 102859

63. ACRIN, The site is funded by the National Cancer Institute's (NCI) Cancer Imaging Program, and the contract is operated by the University of Arkansas for Medical Sciences, 2020.
[Online]. Available: <https://wiki.cancerimagingarchive.net/pages/viewpage.action?pageId=50135264#1619a826e02b4ce8b09f6214aca48665>
64. Rai, Swati, Jignesh S. Bhatt, and S. K. Patra. "An unsupervised deep learning framework for medical image denoising." *arXiv preprint arXiv:2103.06575* (2021)
65. David H. Ackley, Geoffrey E. Hinton, and Terrence J. Sejnowski. A learning algorithm for Boltzmann machines. *Cognitive Science*, 9:147–169, 1985.
66. Lahmiri, S. (2017). An iterative denoising system based on Wiener filtering with application to biomedical images. *Optics & Laser Technology*, 90, 128-132.
67. Krissian, K., & Aja-Fernández, S. (2009). Noise-driven anisotropic diffusion filtering of MRI. *IEEE transactions on image processing*, 18(10), 2265-2274.
68. Lysaker, M., Lundervold, A., & Tai, X. C. (2003). Noise removal using fourth-order partial differential equation with applications to medical magnetic resonance images in space and time. *IEEE Transactions on image processing*, 12(12), 1579-1590.
69. Korolija, s., tuba, e., & tuba, m. *An algorithm for medical magnetic resonance image non-local means denoising*. Infinite study
70. Lin, Y. J., & Chang, H. H. (2015). Automatic Noise Removal in MR Images Using Bilateral Filtering Associated with Artificial Neural Networks.”
71. Wong, W. C., Chung, A. C., & Yu, S. C. (2004, April). Trilateral filtering for biomedical images. In *Biomedical Imaging: Nano to Macro, 2004. IEEE International Symposium on* (pp. 820-823). IEEE.
72. Eskicioglu and P. Fisher, “Image quality measures and their performance,” *IEEE Tr. Comm.*, vol. 43, no. 12, pp. 2959–2965, Dec. 1995
73. D.L.Donoho and I.M.Johnstone, Adapting to unknow smoothness via wavelet shrinkage, *Journal of the American Statistical Association*, vol.90, no.432, pp. 1200-1224, December 1995
74. Starck, J. L., Candès, E. J., & Donoho, D. L. (2002). The Curvelet transform for image denoising. *IEEE Transactions on image processing*, 11(6), 670-684.

75. Misra, Debajyoti, et al. "Effect of using genetic algorithm to denoise MRI images corrupted with Rician Noise." *Emerging Trends in Computing, Communication and Nanotechnology (ICE-CCN), 2013 International Conference on*. IEEE, 2013.
76. Korolev, S., Safiullin, A., Belyaev, M., & Dodonova, Y. (2017, April). Residual and plain convolutional neural networks for 3D brain MRI classification. In *Biomedical Imaging (ISBI 2017), 2017 IEEE 14th International Symposium on* (pp. 835-838). IEEE.
77. Zhang, F., & Ma, L. (2010, October). MRI denoising using the anisotropic coupled diffusion equations. In *Biomedical Engineering and Informatics (BMEI), 2010 3rd International Conference on* (Vol. 1, pp. 397-401). IEEE.
78. Sharif, M., Jaffar, M. A., & Mahmood, M. T. (2014). Optimal composite morphological supervised filter for image denoising using genetic programming: application to magnetic resonance images. *Engineering Applications of Artificial Intelligence*, 31, 78-89.
79. Rajan, Jeny&Jeurissen, Ben &Verhoye, Marleen &Audekerke, Johan &Sijbers, Jan. (2011). Maximum likelihood estimation-based denoising of magnetic resonance images using restricted local neighborhoods. *Physics in medicine and biology*. 56. 5221-34. 10.1088/0031-9155/56/16/009.
80. Sudeep, P. V., et al. "Nonlocal linear minimum mean square error methods for denoising MRI." *Biomedical Signal Processing and Control* 20 (2015): 125-134.
81. K. Dabov, A. Foi, V. Katkovnik and K. Egiazarian, "Image Denoising by Sparse 3-D Transform-Domain Collaborative Filtering," in *IEEE Transactions on Image Processing*, vol. 16, no. 8, pp. 2080-2095, Aug. 2007
82. Maggioni, M., Katkovnik, V., Egiazarian, K., &Foi, A. (2012). Nonlocal transform-domain filter for volumetric data denoising and reconstruction. *IEEE transactions on image processing*, 22(1), 119-133.
83. Baselice, F., Ferraioli, G., Pascazio, V., &Sorriso, A. (2019). Denoising of MR images using Kolmogorov-Smirnov distance in a Non Local framework. *Magnetic resonance imaging*, 57, 176-193.
84. Luisier, F., & Wolfe, P. J. (2011, September). Chi-square unbiased risk estimate for denoising magnitude MR images. In *2011 18th IEEE International Conference on Image Processing* (pp. 1561-1564). IEEE.

85. Abdou, M. A., & Darwish, S. H. (2017). Dual Tree Complex Wavelet with Adaptive Decision Based Median Filter for Medical Image Restoration. *IJCSIS*, 15(4).
86. Dey, N.; Ashour, A.S.; Beagum, S.; Pistola, D.S.; Gospodinov, M.; Gospodinova, E.P.; Tavares, J.M.R.S. Parameter Optimization for Local Polynomial Approximation based Intersection Confidence Interval Filter Using Genetic Algorithm: An Application for Brain MRI Image De-Noiseing. *J. Imaging* **2015**, 1, 60-84.
87. Saluja, R., & Boyat, A. (2015, September). Wavelet based image denoising using weighted highpass filtering coefficients and adaptive wiener filter. In *2015 International Conference on Computer, Communication and Control (IC4)* (pp. 1-6). IEEE.
88. Gupta, M., Taneja, H., & Chand, L. (2018). Performance enhancement and analysis of filters in ultrasound image denoising. *Procedia computer science*, 132, 643-652.
89. Elhoseny, M., & Shankar, K. (2019). Optimal bilateral filter and convolutional neural network based denoising method of medical image measurements. *Measurement*, 143, 125-135
90. Jain, A., & Nahar, P. (2013). Performance Comparison of Two Image Denoising Algorithm at Different Noises. *International Journal of Emerging Technology and Advanced Engineering*, 3(12).
91. Buades, T., Lou, Y., Morel, J. M., & Tang, Z. (2009, August). A note on multi-image denoising. In *2009 International Workshop on Local and Non-Local Approximation in Image Processing* (pp. 1-15). IEEE.
92. Mohan, M. M., Sulochana, C. H., & Latha, T. (2015, March). Medical image denoising using multistage directional median filter. In *2015 International Conference on Circuits, Power and Computing Technologies [ICCPCT-2015]* (pp. 1-6). IEEE.
93. Sara, U., Akter, M., & Uddin, M. S. (2019). Image quality assessment through FSIM, SSIM, MSE and PSNR—a comparative study. *Journal of Computer and Communications*, 7(3), 8-18.
94. Rajalaxmi, S., & Nirmala, S. (2012, December). Echocardiographic image denoising and objective fidelity criteria estimation using entropy paramounted linear regression filter. In *2012 International Conference on Emerging Trends in Science, Engineering and Technology (INCOSET)* (pp. 536-541). IEEE..

95. Hashimoto, F., Ohba, H., Ote, K., Teramoto, A., & Tsukada, H. (2019). Dynamic PET image denoising using deep convolutional neural networks without prior training datasets. *IEEE Access*, 7, 96594-96603.
96. Shahmoradi, M., Lashgari, M., Rabbani, H., Qin, J., & Swain, M. (2016). A comparative study of new and current methods for dental micro-CT image denoising. *Dentomaxillofacial Radiology*, 45(3), 20150302.
97. Chen, L. L., Gou, S. P., Yao, Y., Bai, J., Jiao, L., & Sheng, K. (2016, November). Denoising of low dose CT image with context-based BM3D. In *2016 IEEE Region 10 Conference (TENCON)* (pp. 682-685). IEEE.
98. Esmaeili, M., Dehnavi, A. M., Rabbani, H., & Hajizadeh, F. (2017). Speckle noise reduction in optical coherence tomography using two-dimensional curvelet-based dictionary learning. *Journal of medical signals and sensors*, 7(2), 86.
99. Jensen, C. T., Liu, X., Tamm, E. P., Chandler, A. G., Sun, J., Morani, A. C., ... & Wagner-Bartak, N. A. (2020). Image quality assessment of abdominal CT by use of new deep learning image reconstruction: initial experience. *American Journal of Roentgenology*, 215(1), 50-57